

Optimum design of lead-rubber bearing system with uncertainty parameters

Fan Jian^{*1}, Long Xiaohong¹ and Zhang Yanping²

¹*School of Civil Engineering and Mechanics, Huazhong University of Science and Technology, Wuhan, China*

²*School of Energy and Power Engineering, Huazhong University of Science and Technology, Wuhan, China*

(Received July 1, 2014, Revised October 2, 2015, Accepted November 24, 2015)

Abstract. In this study, a non-stationary random earthquake Clough-Penzien model is used to describe earthquake ground motion. Using stochastic direct integration in combination with an equivalent linear method, a solution is established to describe the non-stationary response of lead-rubber bearing (LRB) system to a stochastic earthquake. Two parameters are used to develop an optimization method for bearing design: the post-yielding stiffness and the normalized yield strength of the isolation bearing. Using the minimization of the maximum energy response level of the upper structure subjected to an earthquake as an objective function, and with the constraints that the bearing failure probability is no more than 5% and the second shape factor of the bearing is less than 5, a calculation method for the two optimal design parameters is presented. In this optimization process, the radial basis function (RBF) response surface was applied, instead of the implicit objective function and constraints, and a sequential quadratic programming (SQP) algorithm was used to solve the optimization problems. By considering the uncertainties of the structural parameters and seismic ground motion input parameters for the optimization of the bearing design, convex set models (such as the interval model and ellipsoidal model) are used to describe the uncertainty parameters. Subsequently, the optimal bearing design parameters were expanded at their median values into first-order Taylor series expansions, and then, the Lagrange multipliers method was used to determine the upper and lower boundaries of the parameters. Moreover, using a calculation example, the impacts of site soil parameters, such as input peak ground acceleration, bearing diameter and rubber shore hardness on the optimization parameters, are investigated.

Keywords: seismic isolated structure; optimal design; lead-core rubber bearing (LRB); stochastic analysis; convex sets

1. Introduction

By providing a seismic bearing between a building and the ground, a base isolation system can reduce the seismic response of the upper structure and therefore block seismic ground motion from passing into the upper structure. Through decades of application, base isolation has become the most widely used technique for controlling and reducing the seismic responses of structures. Generally, an isolation bearing must have a lower lateral stiffness to prolong the resonance period

*Corresponding author, Associate Professor, E-mail: fan-jian@126.com

and reduce the lateral seismic action. In addition, an isolation bearing needs to have appropriate energy dissipation and high restoration ability to avoid excessive bearing displacement and instability. Numerous studies have shown that the mechanical properties of a bearing will greatly affect its seismic abilities. Thus, in recent years, the optimum design of mechanical parameters for isolation bearings has attracted the attention of researchers in a series of studies.

The following studies are representative of some of the previous work. Constantinou and Tadjbakhsh (1984) studied the optimal design of isolated structures containing a mixture of rubber bearings and friction bearings, and their study revealed that a small number of friction units can effectively increase the performance of isolated structures. Park and Otsuka (1999) calculated a linear variation function of optimized yield strength for the bearings in bridge isolated structures facing an intense earthquake, targeting the maximum energy response of the bearing. However, this function was calculated based on a single seismic wave, and thus, it is not suitable for bearing isolated structure optimization design for situations involving different frequencies of ground motions. Zou (2008) proposed a method for optimizing the design values of a concrete base isolated structure based its isolation performance. To obtain the most economical design for the reinforced concrete isolated structure, they simultaneously optimized the upper part of the structure and the seismic isolation devices as a whole, and they used the total cost of the isolated structure under multi-level seismic ground motion as the objective function and specified the maximum inter-story displacement of the upper structure and the bearing horizontal displacement to be less than a certain limit as a constraint. Iemura *et al.* (2007) discussed optimal design of a resilient sliding isolation (RSI) system for the protection of equipment inside buildings. The study found that in the context of minimizing bearing displacement and floor acceleration, greater input peak ground acceleration or smaller optimal bearing stiffness after yielding leads to greater optimal yield strength. Using the maximum isolator displacement (MID) and maximum isolator force (MIF) as targets, Diclel and Karalar (2011) conducted many nonlinear time history (NLTH) analyses on representative bridges. They obtained an analytical formula for optimum bearing strength and optimal stiffness after yielding by nonlinear fitting analysis methods. This analytical formula included the effects of bearings, bridge structures and input seismic ground motion characteristics. Using this formula, by selecting the appropriate bearing mechanical parameters, designers can obtain economical and robust design of bridge seismic isolation. Islam *et al.* (2012) provided incorporation of lead rubber bearing and high damping rubber bearing as base isolators, nonlinear dynamic time domain analyses were performed for both isolated and non-isolated buildings under site specific bi-directional earth-Bi-directional earthquake. The study reveals that for medium rise building construction, isolation can significantly reduce seismic response in soft to medium stiff soil. In accordance with Pareto-type optimization principles that solve multi-objective functions with competing objectives, Bucher (2009) optimized the design parameters of the bearings in a frictional isolated structure based on probability. The objective function can be expressed as the cost function of maximum bearing displacement, residual bearing displacement, and maximum upper structure inter-story displacement. The optimization process used the moving least squares (MLS) objective function as a response surface, based on Latin hypercube sampling, to explicitly express the objective function. Pourzeynali and Zarif (2008) optimized the design of upper-level isolated structures using multi-objective optimization. In this design, the base mass, stiffness, and damping ratio were used as design variables, and the minimization of the displacement of the top portion of the structure and the minimization of bearing displacement were used as objectives. Because these two objective functions are mutually contradictory, a fast and efficient Non-dominated Sorting Genetic Algorithm (NSGA-II) was used

to solve the Pareto optimization problem. Ultimately, the optimum values of the design variables for the seismic isolated structure under a deterministic earthquake ground effect were obtained. Ozbulut and Hurlebaus (2011) studied the optimal design of super-elastic friction seismic isolation for continuous girder bridges. Using the isolation girder natural frequency, the yield displacement of Shape Memory Alloy (SMA) devices, and the friction coefficient of the sliding bearings as design variables, they used sensitivity analysis on the bearing design parameters to obtain the optimal values of the parameters. Jangid (2008) studied parameter optimization for lead-rubber bearings (LRB) and a friction pendulum system (FPS) of isolation girder bridges under random white noise excitation from the ground. Using the minimum an-squared value of acceleration on the bridge surface as the objective function, the author proposed analytic formulas for the calculation of optimal bearing yield strength or optimum friction coefficients. The formula is a function of the power spectral density constant, the damping ratio of the structure and the post-yielding stiffness of the bearing. Furthermore, the parameter values of the seismic isolation bearings of LRB and FPS structures under the influence of near-field ground motions were calculated (Jangid 2005, 2007). The results showed that under the influence of near-field ground motions, the optimum bearing yield strength or bearing friction coefficient should be 10%-15% of the total mass of the structure. Baratla and Corbi (2004) simulated the input seismic ground motion using a stationary stochastic process with the Kanai-Tajimi power spectral density function, and they explored the optimal design of multi-storey structures using frequency-domain analysis of random vibration. Using the elastic stiffness of the bearings and foundation mass as optimization design variables and the minimum energy absorbed by the upper structure as the objective function, they calculated the optimal values for isolated structure bearing stiffness for different categories of site soil. However, the limitation of this paper is the use of linear elements to simulate isolation bearings, non-linear elements are more commonly used for isolation bearings in actual projects.

All of the aforementioned studies do not take into account the effects of structural parameter uncertainties on the optimal design of isolated structures. Existing literature suggests that the interaction between the uncertainty of structural parameters and the uncertainty of the load will significantly affect the structural dynamic response (Jensen 2005) and safety of a structure (Chaudhuri and Chakraborty 2004), as well its optimal design (Schueller and Jensen 2008). Mishra and Chakraborty (2013), Mishra *et al.* (2013) took into account the combined effect of the uncertainties of structural parameters and input ground motion, and they used a reliability-based optimization method for the optimized design of isolated structures. Based on a matrix perturbation method and the first-order Taylor expansion, they applied the total probability theory to determine the structural response to a stochastic earthquake, with consideration of the uncertainty of the structural parameters. Subsequently, by minimizing the non-conditional probability of failure of the upper structure, they obtained the optimal value of the normalized yield strength of the isolation bearing. Recently, they also applied this method for the multi-objective stochastic optimization design for friction isolated structures with SMA devices (Gur and Mishra 2013).

In this paper, a non-stationary Clough-Penzien random seismic model is used to describe earthquake ground excitation. Furthermore, using a stochastic direct integration method combined with the equivalent linear method, a solution for the non-stationary seismic response of a lead-rubber bearing (LRB) system under the effects of a stochastic earthquake is proposed. Two parameters are adopted for the development of an optimal bearing design: post-yielding stiffness and normalized yield strength. Using the minimum value of the maximum energy response level of

the upper structure subjected to an earthquake as an objective function, and with the constraints that the bearing failure probability should be no more than 5% and the second shape factor of the bearing should be less than 5, the optimal values are calculated for the two design parameters. In this optimization process, the radial basis function (RBF) is used instead of the implicit objective function and constraints, and a sequential quadratic programming (SQP) algorithm is used to solve the optimization problems. With consideration of the uncertainties of the structural parameters and seismic ground motion input parameters in the optimization of the bearing design, convex set models (such as the interval model and ellipsoidal model) are used to describe the uncertainty parameters. Subsequently, the optimal bearing design parameters were expanded at their median values into first-order Taylor series expansions, and a Lagrange multiplier method was used to determine the upper and lower boundaries of the parameters.

2. An input seismic ground motion model

A non-stationary Clough-Penzien stochastic seismic model (Clough and Penzien 1977) is used to describe earthquake excitation $a_g(t)$

$$\begin{aligned}
 a_g(t) &= -\omega_f^2 x_f(t) - 2\zeta_f \omega_f \dot{x}_f(t) + \omega_g^2 x_g(t) + 2\zeta_g \omega_g \dot{x}_g(t) \\
 \ddot{x}_f(t) + \omega_f^2 x_f(t) + 2\zeta_f \omega_f \dot{x}_f(t) &= \omega_g^2 x_g(t) + 2\zeta_g \omega_g \dot{x}_g(t) \\
 \ddot{x}_g(t) + 2\zeta_g \omega_g \dot{x}_g(t) + \omega_g^2 x_g(t) &= -a(t)w(t)
 \end{aligned}
 \tag{1}$$

where $x_g(t)$ and $x_f(t)$ are the responses of the filter, ω_f , ω_g are the characteristic frequencies of the filter, ζ_f and ζ_g are the filter damping ratios, $w(t)$ is the white noise when the power spectral intensity is S_0 , $a(t)$ is the time modulation function given by the following equation (Marano *et al.* 1968)

$$a(t) = \begin{cases} (t/t_1)^2 & 0 \leq t \leq t_1 \\ 1 & t_1 \leq t \leq t_2 \\ e^{-c(t-t_2)} & t \geq t_2 \end{cases}
 \tag{2}$$

The peak acceleration of ground motion PGA is $3\sigma_{a_g}$, so the relationship between S_0 and PGA can be written as (Marano *et al.* 2011)

$$S_0 = \frac{0.222}{\pi} \frac{PGA^2 \zeta_g^2 \zeta_f^2 \left((\omega_g^4 + 4\zeta_g \zeta_f \omega_g^3 \omega_f + 2(-1 + 2\zeta_g^2 + 2\zeta_f^2) \omega_g^2 \omega_f^2 + 4\zeta_g \zeta_f \omega_g \omega_f^3 + \omega_f^4) \right)}{\omega_g^2 ((1 + 4\zeta_g^2) \zeta_f \omega_g^3 + \zeta_g (1 + 16\zeta_g^2 \zeta_f^2) \omega_g^2 \omega_f + 16\zeta_g^4 \zeta_f \omega_g \omega_f^2 + 4\zeta_g^3 \omega_f^4)}
 \tag{3}$$

Table 1 lists values of these seismic model parameters in different field types.

3. The motion equation

The nonlinear motion equation for the multi-degree-of-freedom lead-rubber bearing system under horizontal seismic excitation $a_g(t)$ can be written as

Table 1 Values of seismic model parameters in different field types.

Field type	v_{sm} (m/s)*	ω_g (rad/s)	ζ_g	ω_f (rad/s)	ζ_f	t_1 (s)	t_2 (s)	C
I	$v_{sm} > 500$	31.42	0.64	4.71	0.64	6.8	12.8	0.12
II	$250 < v_{sm} \leq 500$	20.92	0.72	3.14	0.72	7.0	13.5	0.11
III	$140 < v_{sm} \leq 250$	15.71	0.80	2.36	0.80	7.5	14.5	0.11
IV	$v_{sm} < 140$	9.67	0.90	1.45	0.90	8.0	15.5	0.10

* v_{sm} : soil equivalent shear wave velocity

$$M_s \ddot{X}_s + C_s \dot{X}_s + K_s X_s = -M_s I (a_g + \ddot{x}_b) \tag{4}$$

$$m_b (a_g + \ddot{x}_b) + \sum_{i=1}^n m_i (\ddot{x}_i + \ddot{x}_b + a_g) + F_Q(x_b, \dot{x}_b) = 0 \tag{5}$$

where M_s , C_s and K_s are the mass, damping and stiffness matrices of the upper structure, m_i is the mass of the i -th floor, $X_s = [x_1, \dots, x_n]^T$ is the displacement of the upper structure relative to the base, m_b is the mass of the base, $I = [1, \dots, 1]^T$, $F_Q(x_b, \dot{x}_b)$ is the hysteretic restoring force of the lead-rubber bearing and x_b is the displacement of the base relative to the ground.

In this paper, $F_Q(x_b, \dot{x}_b)$ is treated as a bilinear model (dashed line in Fig. 1). Because the pre-yielding stiffness of the LRB is 10 - 15 times its post-yielding stiffness, under the condition of equal hysteresis area, the bilinear restoring force model simplifies to a rigid-plastic model (solid line in Fig. 1). Thus, $F_Q(x_b, \dot{x}_b)$ can be expressed as (Jangid 2008)

$$F_Q(x_b, \dot{x}_b) = N\alpha k_b x_b + N(1 - \alpha) f_y \text{sign}(\dot{x}_b) \tag{6}$$

where N is the total number of isolation bearings, k_b is the pre-yielding stiffness of the bearing, f_y is the yield force of the bearing and α is the ratio of pre-yielding and post-yielding stiffness.

Based on a random equivalent linearization method, Eq. (6) can be replaced with a linear equation, that is (Jangid 2008)

$$F_Q(x_b, \dot{x}_b) = N\alpha k_b x_b + N(1 - \alpha) f_y c_e(t) \dot{x}_b \tag{7}$$

where $c_e(t)$ is the equivalent time-varying damping coefficient, which can be calculated as

$$c_e(t) = \frac{1}{\sigma_{\dot{x}_b}(t)} \sqrt{\frac{2}{\pi}} \tag{8}$$

In Eq. (8), $\sigma_{\dot{x}_b}(t)$ is the time-varying standard deviation of \dot{x}_b .

Eq. (7) is substituted into Eq. (5) to yield the following equation

$$\sum_{i=1}^n r_i \ddot{x}_i + \ddot{x}_b + \omega_b^2 x_b + \mu g c_e(t) \dot{x}_b = -a_g(t) \tag{9}$$

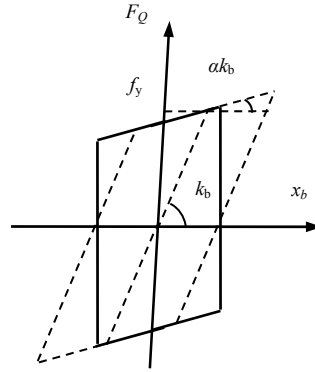


Fig. 1 Hysteretic restoring force model of lead-rubber bearings

In this equation, $r_i = \frac{m_i}{M_z}$, $M_z = \sum_{i=1}^n m_i + m_b$ is the total mass of the isolated structure, $\omega_b = \frac{N\alpha k_b}{M_z}$, $\mu = \frac{N(1-\alpha)f_y}{M_z g}$ is the ratio of yield force to the mass of the isolated structure and two parameters (ω_b and μ) determine the stiffness k_b and yield force f_y of the bearing.

Combining Eqs. (4) and (9), the equivalent linear motion equation can be written as

$$M\ddot{X} + C\dot{X} + KX = -I_m a_g(t) \tag{10}$$

In this equation, $M = \begin{bmatrix} M_s & \begin{Bmatrix} m_1 \\ \vdots \\ m_n \end{Bmatrix} \\ \{r_1, r_2, \dots, r_n\} & 1 \end{bmatrix}_{n+1}$, $C = \begin{bmatrix} C_s & 0 \\ 0 & \mu g c_e \end{bmatrix}$, $K = \begin{bmatrix} K_s & 0 \\ 0 & \omega_b \end{bmatrix}$,

$I_m = \{m_1, \dots, m_n, 1\}'$, and $X = \{x_1, \dots, x_n, x_b\}'$.

Combining Eq. (10) with Eq. (1), which is a differential equation describing seismic excitation, and introducing a state variable, $Y = \{X, x_f, x_g, \dot{X}, \dot{x}_f, \dot{x}_g\}'$, the state equation can be obtained as

$$\dot{Y}(t) = A_e(t)Y(t) + F(t) \tag{11}$$

The formulae of $F(t)$ and $F_e(t)$ are described in the Appendix.

4. Stochastic analysis method

With consideration of the time-varying character of $A_e(t)$ in Eq. (11), time t is subdivided into a finite number of equally spaced moments separated by Δt : $t=0, \Delta t, \dots, n\Delta t, (n+1)\Delta t, \dots$. Within the

n -th time period $\tau \in [n\Delta t, (n+1)\Delta t]$, $A_e(\tau)$ is assumed to be approximately constant. In addition, let $A_e(\tau) = A_{er}(\tau) = rA_e(n) + (1-r)A_e(n+1)$, where r represents the relative weight of $A_e(n)$. Assuming that the external load exhibits linear variation, i.e., $F(\tau) = F(n) + \frac{F(n+1) - F(n)}{\Delta t}(\tau - n\Delta t)$, the state equation, Eq. (11), can be simplified within this period to

$$\dot{Y}(\tau) = A_{er}(n)Y(\tau) + F(\tau) \tag{12}$$

Solving Eq. (12), $Y(n+1)$ within $(n+1)\Delta t$ could be obtained as

$$Y(n+1) = B_1(n)Y(n) + B_2(n)F(n) + B_3(n)F(n+1) \tag{13}$$

Where $B_1(n) = \exp(A_{er}(n)\Delta t)$, $B_2(n) = (B_1(n) - I)A_{er}^{-1}(n) - \frac{B(n)}{\Delta t}$, $B_3(n) = \frac{B(n)}{\Delta t}$ and $B(n) = B_1(n)(A_{er}^{-1}(n))^2 - (A_{er}^{-1}(n)) - A_{er}^{-1}(n)\Delta t$.

To obtain the mean response, the average on both sides of Eq. (13) is taken

$$E[Y(n+1)] = B_1(n)E[Y(n)] + B_2(n)E[F(n)] + B_3(n)E[F(n+1)] \tag{14}$$

Because $w(t)$ is the white noise input, both $E[F(n)]$ and $E[F(n+1)]$ in Eq. (14) are zero. Thus, Eq. (14) can be rewritten as follows

$$E[Y(n+1)] = B_1(n)E[Y(n)] = \prod_{i=0}^n B_1(i)E[Y(0)]$$

With zero initial condition, $E[Y(n+1)] = 0$ could be obtained.

The auto correlation matrix of $Y(n+1)$ is

$$\begin{aligned} R[Y(n+1)] &= E[Y(n+1)Y^T(n+1)] \\ &= B_1(n)R[Y(n)]B_1^T(n) + B_1(n)E[Y(n)F^T(n)]B_2^T(n) + B_1(n)E[Y(n)F^T(n+1)]B_3^T(n) \\ &+ B_2(n)E[F(n)Y^T(n)]B_1^T(n) + B_2(n)R[F(n)]B_2^T(n) + B_2(n)E[F(n)F^T(n+1)]B_3^T(n) \\ &+ B_3(n)E[F(n+1)Y^T(n)]B_1^T(n) + B_3(n)E[F(n+1)F^T(n)]B_2^T(n) + B_3(n)R[F(n+1)]B_3^T(n) \end{aligned} \tag{15}$$

Next, under the condition that $E[F(n)F^T(n+1)]$, $E[F(n+1)F^T(n)]$, $E[Y(n)F^T(n+1)]$ and $E[F(n+1)Y^T(n)]$ are all equal to zero, Eq. (15) becomes

$$\begin{aligned} R[Y(n+1)] &= B_1(n)R[Y(n)]B_1^T(n) + B_1(n)E[Y(n)F^T(n)]B_2^T(n) + B_2(n)E[F(n)Y^T(n)]B_1^T(n) \\ &+ B_2(n)R[F(n)]B_2^T(n) + B_3(n)R[F(n+1)]B_3^T(n) \end{aligned} \tag{16}$$

where

$$E[Y(n)F^T(n)] = B_1(n-1)E[Y(n-1)F^T(n)] + B_2(n-1)E[F(n-1)F^T(n)] + B_3(n-1)R[F(n)]$$

Because $E[Y(n-1)F^T(n)]$ and $E[F(n-1)F^T(n)]$ are zero, the above equation becomes

$$E[Y(n)F^T(n)] = B_3(n-1)R[F(n)] \tag{17}$$

Similarly

$$E[F(n)Y^T(n)] = R[F(n)]B_3^T(n-1) \tag{18}$$

Substituting Eq.s (17) and (18) into Eq. (16) gives

$$R[Y(n+1)] = B_1(n)R[Y(n)]B_1^T(n) + B_1(n)B_3(n-1)R[F(n)]B_2^T(n) + B_2(n)R[F(n)]B_3^T(n-1)B_1^T(n) + B_2(n)R[F(n)]B_2^T(n) + B_3(n)R[F(n+1)]B_3^T(n) \tag{19}$$

In the above equation, the $2(n+3) \times 2(n+3)$ -th element of $R[F(n)]$ and $R[F(n+1)]$ has a value of $2\pi S_0 a^2(n)/\Delta t$ and $2\pi S_0 a^2(n+1)/\Delta t$ respectively, but all other elements are zero. With the initial condition $R[Y(0)]=0$, $R[Y(t)]$ can be calculated for different time points. Note that when $r=1$, Eq. (19) does not need to be solved iteratively, when $r \neq 1$, an iterative solution is needed.

5. Optimal bearing designs with deterministic structural parameters

Based on Eq. (9), it can be seen that ω_b and μ determine the post-yielding stiffness and yield force. Therefore, ω_b and μ are use as optimization parameters in this study. The objective function is set to minimize the ratio of the maximum energy responses in the upper structure with and without seismic isolation under the influence of an earthquake. The mathematical expression is

Find ω_b, μ

$$\min f_{obj}(\omega_b, \mu) = \frac{E_{str}^b}{E_{str}^f} = \frac{\sum_{i=1}^n \max_{t \in [0, T]} [\sigma_b^2(x_i, t)]}{\sum_{i=1}^n \max_{t \in [0, T]} [\sigma_f^2(x_i, t)]} \tag{20}$$

In this equation, $\sigma_b^2(x_i, t)$ is $E[x_i^2(t)]$ when the base is seismically isolated, and $\sigma_f^2(x_i, t)$ is $E[x_i^2(t)]$ when the base is fixed; both values can be calculated by using stochastic direct integration.

While satisfying the above objective function, the following two constraint conditions also need to be satisfied:

Constraint condition 1: The probability of the horizontal displacement of the isolation bearing exceeding the allowable limit under the seismic effect is less than 5%. Mathematically, this is expressed as

$$F^b(\omega_b, \mu) = 1 - \min_{t \in [0, T]} r(t) \leq 5\% \tag{21}$$

In this equation, $r(t) = \exp\left\{-\int_0^t 2v'_b(b, \tau) d\tau\right\}$, and $v'_b(b, \tau)$ is expressed as follows (Vanmarcke 1975)

$$v'_b(b, \tau) = \frac{1}{\pi} \frac{\sigma_{\dot{x}_b}(t)}{\sigma_{x_b}(t)} \left(\frac{1 - \exp\left(-\sqrt{\frac{\pi}{2}} \frac{b(q(t))^{1/2}}{\sigma_{x_b}(t)}\right)}{\exp\left(\frac{1}{2} \left(\frac{b}{\sigma_{x_b}(t)}\right)^2\right) - 1} \right) \tag{22}$$

Here, b is the allowable displacement limit. According to the seismic code of China, $b = \min[0.55D, 300\%ntr]$, where D is the bearing diameter, ntr is the total thickness of the rubber in the bearing, $\sigma_{x_b}(t) = \sqrt{E[x_b^2(t)]}$, $\sigma_{\dot{x}_b}(t) = \sqrt{E[\dot{x}_b^2(t)]}$ and $q(t)$ is a bandwidth parameter that can be expressed as follows:

$$q(t) = \sqrt{1 - \frac{\lambda_1^2(t)}{\lambda_0(t)\lambda_2(t)}}$$

In this expression, $\lambda_0(t) = E[x_b^2(t)]$, $\lambda_1(t) = E[x_b(t)\dot{x}_b(t)]$, and $\lambda_2(t) = E[\dot{x}_b^2(t)]$.

As shown in the following equation, ntr is related to the second stiffness, $k_2 = \alpha k_b$, of a single bearing

$$Nk_2 = GA / ntr \tag{23}$$

Here, N is the total number of isolation bearings, G is the shear modulus of the rubber, $A = P_d / [\sigma_b]$ is the total area of all bearings, P_d is the total vertical design load, and $[\sigma_b]$ is the allowable stress of the bearing design, usually 10-15 MPa.

By substituting $A = P_d / [\sigma_b]$ into Eq. (23) gives:

$$Nk_2 = \frac{GP_d}{ntr[\sigma_b]}$$

Then, after dividing both sides of the above equation by the total mass of the structure, the following equation is obtained

$$\frac{Nk_2}{M_z} = \frac{GP_d}{ntr \cdot M_z[\sigma_b]} = \frac{GP_d g}{ntr \cdot G_z[\sigma_b]} = \frac{G\beta g}{ntr[\sigma_b]} \tag{24}$$

Here, $G_z = M_z g$ is the representative value of gravity load in the structure, and $\beta = P_d / G_z$ is a number greater than 1.

Because $\frac{Nk_2}{M_z} = \omega_b^2$, Eq. (24) can be converted to

$$ntr = \frac{G\beta g}{\omega_b^2[\sigma_b]} \tag{25}$$

Based on Eq. (25), it can be seen that b in Eq. (22) is a function of ω_b , and when ω_b is determined, the total rubber thickness in the bearing, ntr , is also determined.

Constraint condition 2: To prevent instability under a vertical load, it is required that the second shape factor, S_2 , of the bearing should be greater than a limiting value m (m usually has a

value of 4 - 6):

$$S_2 = \frac{D}{ntr} \geq m$$

By substituting Eq. (25) into the above equation gives

$$S_2(\omega_b, \mu) = \frac{D}{ntr} = \frac{D\omega_b^2[\sigma_b]}{G\beta g} \geq m \tag{26}$$

Combining Eqs. (20), (21) and (26), a mathematical model of optimized bearing parameters can be obtained as

$$\begin{aligned} & \text{Find } \omega_b, \mu \\ & \min f_{obj}(\omega_b, \mu) \\ & \text{s.t. } \mathbf{F}^b(\omega_b, \mu) \leq 5\% \\ & \quad S_2(\omega_b, \mu) \geq m \end{aligned} \tag{27}$$

In the process of solving Eq. (27), because $f_{obj}(\omega_b, \mu)$ and $\mathbf{F}^b(\omega_b, \mu)$ are implicit functions of ω_b, μ , the computational efficiency would be very low if it is solved directly, resulting in not only long computation times but also non-convergent results. To improve the computational efficiency, an RBF response surface is used to make $f_{obj}(\bullet)$ and $\mathbf{F}^b(\bullet)$ explicit (Fang and Horstemeyer 2006, McDonald *et al.* 2007). Here, $f_{obj}(\bullet)$ is taken as an example:

$$f_{obj}(\mathbf{x}) \approx \tilde{f}_{obj}(\mathbf{x}) = \sum_{j=1}^n \lambda_j \varphi(\|\mathbf{x} - \mathbf{x}^j\|) \tag{28}$$

In this equation, $\mathbf{x}=[x_1, x_2]=[\omega_b, \mu]$, n is the number of interpolation sample points, \mathbf{x}^j is j -th interpolation sample point vector, λ_j is the coefficient to be solved for, $\varphi(\|\mathbf{x}-\mathbf{x}^j\|)$ is the RBF and $\|\mathbf{x}-\mathbf{x}^j\|$ is the distance between any \mathbf{x} and the j -th interpolation point and is given by the following expression:

$$\|\mathbf{x} - \mathbf{x}^j\| = \sqrt{(x_1 - x_1^j)^2 + (x_2 - x_2^j)^2}$$

For the convenience of expression, let $r^{oj}=\|\mathbf{x}-\mathbf{x}^j\|$ and $r^{ij}=\|\mathbf{x}^i-\mathbf{x}^j\|$.

If there are n interpolation sample points, then, based on Eq. (28), $\tilde{f}_{obj}(\mathbf{x})$ can be expressed as

$$\tilde{f}_{obj}(\mathbf{x}^i) = \sum_{j=1}^n \lambda_j \varphi(r^{ij}) \quad (i = 1, 2, \dots, n) \tag{29}$$

Where $\varphi(\bullet)$ is the RBF, and let it to be Gaussian in this paper: $\varphi(r) = e^{-cr^2}$.

Eq. (29) is a set of linear equations for λ_j ($j=1,2,\dots,n$). Values of λ_j can be obtained by solving

Eq. (29). Substituting λ_j into Eq. (28), an approximate explicit expression of $f_{obj}(\mathbf{x})$ and $\tilde{f}_{obj}(\mathbf{x})$ can be obtained. Similarly, the approximate explicit expression of $F^b(\mathbf{x})$ in the constraint condition 1, $\tilde{F}^b(\mathbf{x})$, can also be obtained. After replacing $f_{obj}(\bullet)$ and $F^b(\bullet)$ in Eq. (27) with $\tilde{f}_{obj}(\bullet)$ and $\tilde{F}^b(\bullet)$ and using an SQP algorithm, the two optimal parameters $\omega_b^{opt}, \mu^{opt}$ can be obtained.

Specifically, the calculation steps are the following:

- 1) A set of interpolation sample points $\mathbf{x}^i = (\omega_b^i, \mu^i), (i = 1, 2, \dots, n)$ is selected.
- 2) The objective response values $\tilde{f}_{obj}(\mathbf{x}^i)$ and constraint response values $\tilde{F}^b(\mathbf{x}^i)$ at every sample point are calculated.
- 3) By substituting $\tilde{f}_{obj}(\mathbf{x}^i)$ into Eq. (29), the set of linear equations can be solved to obtain λ_j , and $\tilde{f}_{obj}(\mathbf{x})$ can then be obtained by substituting λ_j into Eq. (28); similarly, $\tilde{F}^b(\mathbf{x})$ can also be obtained.
- 4) After the substitution of $\tilde{f}_{obj}(\mathbf{x})$ and $\tilde{F}^b(\mathbf{x})$ into Eq. (27), the SQP algorithm is used to solve the optimization problem. In the process of obtaining the solution, the interpolation sample point that satisfies the constraint conditions and has the smallest object response value is selected as the initial point for SQP.
- 5) The convergence tolerance is detected. Solving is completed if the convergence tolerance is satisfied; otherwise, the current optimization result is used as an initial point and, as a new sample point, is added to the original sample points to re-build and re-solve a new model. The process is repeated until the current result and the results of previous iterations satisfy the convergence tolerance criteria. Finally, the optimized bearing parameters $\mathbf{x}^{opt} = [\omega_b^{opt}, \mu^{opt}]$ are obtained.

6. Optimal bearing design with the consideration of parametric uncertainty

6.1 Description of uncertainty parameters

In actual engineering practice, there are uncertainties associated with structural parameters and input seismic ground motion parameters. These uncertainties will affect the optimal design of the isolation bearing. Models describing parametric uncertainty include the probabilistic model, which is established based on statistics, and the non-probabilistic convex model, which has been developed in recent years and is based on convex set theory. The probabilistic model requires a large number of samples, or relies on the repeatability of events, to obtain complete information about the probability distribution. However, in practice, it is usually difficult to obtain a large amount of statistical data. In contrast, even if there is a small amount of uncertainty information available, with an unknown probability distribution function, the non-probabilistic convex model can identify the amplitude or the boundaries of the parameter uncertainties based on the available information. Furthermore, this model can describe the boundaries using convex sets, such as the interval set or ellipsoidal set (Ellishakoff 1995, Ben-Haim 1994, Qiu and Wang 2010). In this paper, the uncertainties of structural parameters and seismic ground motion input parameters are described by the interval model and ellipsoidal model. Specifically, the uncertainty vector is $\mathbf{X} = [\mathbf{K}_s, \mathbf{M}_s, m_b, \omega_f, \zeta_f, \omega_g, \zeta_g, S_0] = [x_1, \dots, x_8]$. According to convex set theory, $x_i \in \mathbf{X}$ can be expressed as

$$\mathbf{x}_i = (1 + \gamma_i \delta_i) \mathbf{x}_i^c \tag{30}$$

Table 2 Chart of uncertainty variables

Uncertainty variable	Average value	Deviation rate (%)	Standardized variable	Convex model description
K	K^c	0-10	δ_1	
M	M^c	0-10	δ_2	$\delta_1^2 + \delta_2^2 \leq 1$
m_b	m_b^c	0-10	δ_2	
ω_g	ω_g^c	0-10	δ_3	
ω_f	ω_f^c	0-10	δ_3	
ξ_g	ξ_g^c	0-10	δ_4	$\delta_3^2 + \delta_4^2 + \delta_5^2 \leq 1$
ξ_f	ξ_f^c	0-10	δ_4	
S_0	S_0^c	0-10	δ_5	

where $x_i^c = \frac{x_i^u + x_i^l}{2}$ is the average value of x_i and γ_i is the deviation rate of x_i . The values x_i^u and x_i^l are the upper and lower bounds of x_i , respectively, and $\delta_i \in [-1,1]$ is a standardized variable.

Table 2 lists the properties of the uncertainty variables. Table 2 shows that M_s and m_b are fully correlated and expressed by the same standardized variable δ_2 . ω_f and ω_g , as well as ξ_f and ξ_g are also fully correlated and expressed as standardized variables: δ_3 and δ_4 , respectively. Therefore, the vector of non-fully correlated standardized variables is $\delta = [\delta_1, \delta_2, \dots, \delta_5]$. If the interval model is used to define δ , δ can be expressed as

$$\delta \in E = \{\delta : \delta_i^2 \leq 1, i = 1, 2, \dots, 5\} \tag{31}$$

If the restrictive relationship among a portion of the uncertainty parameters is taken into account, and if the ellipsoidal model can be used to define δ , then

$$\delta \in E = \left\{ \delta : \{\delta_1, \delta_2\} \begin{Bmatrix} \delta_1 \\ \delta_2 \end{Bmatrix} \leq 1, \{\delta_3, \delta_4, \delta_5\} \begin{Bmatrix} \delta_3 \\ \delta_4 \\ \delta_5 \end{Bmatrix} \leq 1 \right\} \tag{32}$$

As shown in Eq. (32), there are correlations between structural parameters and between seismic ground motion parameters, but the structural parameters are independent of the seismic ground motion parameters.

6.2 Bearing design optimization with the consideration of uncertainty

If the uncertainties of structural parameters are taken into account, the optimization parameters ω_b^{opt} and μ^{opt} of the bearings become functions of δ . Because δ varies within the convex domain of Eq. (31) or (32), both $\omega_b^{opt}(\delta)$ and $\mu^{opt}(\delta)$ should be variables with boundaries and given by the following equation

$$\begin{aligned} \omega_{b,\max}^{opt} &= \sup_{\delta \in E} \{\omega_b^{opt}(\delta)\}, & \mu_{\max}^{opt} &= \sup_{\delta \in E} \{\mu^{opt}(\delta)\} \\ \omega_{b,\min}^{opt} &= \inf_{\delta \in E} \{\omega_b^{opt}(\delta)\}, & \mu_{\min}^{opt} &= \inf_{\delta \in E} \{\mu^{opt}(\delta)\} \end{aligned} \tag{33}$$

Where $\omega_{b,\max}^{opt}$ and μ_{\max}^{opt} , and $\omega_{b,\min}^{opt}$ and μ_{\min}^{opt} are the upper and lower bounds of ω_b^{opt} and μ^{opt} , respectively.

Therefore, $\omega_b^{opt}(\delta)$ and $\mu^{opt}(\delta)$ are variables with a limited range:

$$\omega_b^{opt}(\delta) \in [\omega_{b,\min}^{opt}, \omega_{b,\max}^{opt}], \quad \mu^{opt}(\delta) \in [\mu_{\min}^{opt}, \mu_{\max}^{opt}]$$

A solution of Eq. (33) can be obtained by solving the following constrained optimization problem (used for solving for $\mu_{\min}^b, \mu_{\max}^b$, for example)

Find δ

$$\begin{aligned} \mu_{\min}^{opt} &= \min(\mu^{opt}(\delta)), \text{ or } \mu_{\max}^{opt} = \max(\mu^{opt}(\delta)) \\ \text{s.t. } \delta_i^2 &\leq 1 \quad (i = 1, 2, \dots, 5) && \text{(Interval model)} \\ \text{s.t. } \delta_1^2 + \delta_2^2 &\leq 1, \delta_3^2 + \delta_4^2 + \delta_5^2 \leq 1 && \text{(Ellipsoidal model)} \end{aligned} \tag{34}$$

In solving Eq. (34), because $\mu^{opt}(\delta)$ is an implicit function of δ , the computational efficiency will be very low if it is solved directly. Taking into account the fact that the deviation rates of uncertainty variables are usually within 10%, $\mu^{opt}(\delta)$ can be expanded into a Taylor series at $\delta=0$, that is

$$\mu^{opt}(\delta) \approx \tilde{\mu}^{opt}(\delta) = \mu^{opt}(0) + \sum_{i=1}^5 \frac{\partial \mu^{opt}(0)}{\partial \delta_i} \cdot \delta_i \tag{35}$$

In Eq. (35), $\frac{\partial \mu^{opt}(0)}{\partial \delta_i}$ can be solved by expressing it in a difference form

$$\frac{\partial \mu^{opt}(0)}{\partial \delta_i} = \frac{\mu^{opt}(\Delta\delta_i) - \mu^{opt}(0)}{\Delta\delta_i} \tag{36}$$

Where $\Delta\delta_i = [0, \dots, \Delta\delta_i, \dots, 0]$, and $\Delta\delta_i$ is the mini-increment.

In Eqs. (35) and (36), $\mu^{opt}(\Delta\delta_i)$ and $\mu^{opt}(0)$ can be obtained by using the deterministic bearing parameter optimization calculation method mentioned in the previous section.

When using an interval model to simulate uncertainty variables, substitute Eq. (35) into Eq. (34) and the following expressions for μ_{\min}^{opt} and μ_{\max}^{opt} can be obtained:

$$\begin{aligned} \mu_{\min}^{opt} &= \mu^{opt}(0) - \sum_{i=1}^5 \text{abs}\left(\frac{\partial \mu^{opt}(0)}{\partial \delta_i}\right) \\ \mu_{\max}^{opt} &= \mu^{opt}(0) + \sum_{i=1}^5 \text{abs}\left(\frac{\partial \mu^{opt}(0)}{\partial \delta_i}\right) \end{aligned} \tag{37}$$

If the ellipsoidal model is used to simulate uncertainty variables, substitute Eq. (35) into Eq. (34) and the analytical expressions for μ_{\min}^{opt} and μ_{\max}^{opt} can be obtained by using a Lagrange multiplier method:

$$\begin{aligned}\mu_{\min}^{opt} &= \mu^{opt}(\mathbf{0}) - \sqrt{\sum_{i=1}^2 \left(\frac{\partial \mu^{opt}(\mathbf{0})}{\partial \delta_i} \right)^2} - \sqrt{\sum_{j=3}^5 \left(\frac{\partial \mu^{opt}(\mathbf{0})}{\partial \delta_j} \right)^2} \\ \mu_{\max}^{opt} &= \mu^{opt}(\mathbf{0}) + \sqrt{\sum_{i=1}^2 \left(\frac{\partial \mu^{opt}(\mathbf{0})}{\partial \delta_i} \right)^2} + \sqrt{\sum_{j=3}^5 \left(\frac{\partial \mu^{opt}(\mathbf{0})}{\partial \delta_j} \right)^2}\end{aligned}\quad (38)$$

7. A calculation example

7.1 Structure description and optimized bearing design

Taking a five-story office building made of reinforced concrete as an example, the plan of the standard floor is rectangular, the short side (x -direction) is 36 m and the long side (y -direction) is 51m, as shown in Fig. 2. The building is located on a type II field (as shown in Table 1). The earthquake ground motion enters in the x -direction, and the ground motion parameters are listed in Table 1. Two conditions are considered for the peak ground acceleration: $PGA=0.5$ g and $PGA=0.8$ g. The basic period of the fixed base in the x -direction is 0.42s, and the lumped mass and the inter-story stiffness of every level in the x -direction are listed in Fig. 2(b). The isolation bearing layout is shown in Fig. 2(a), with a total of 40 lead-core rubber bearings that have a diameter (D) of 0.7 m. If the bearing rubber has a shore hardness of 45 degrees, and the shear modulus G is 0.54 MPa, then the second shape factor of the bearing is $S_2 \geq m=5$. With $\beta=1.3$, the average stress of the bearing is $\sigma = P_d/A = \beta M_z g / (40A_b) = 10.6$ Mpa (40 is the total number of isolation bearings, A_b is the area of a single bearing).

This base-isolated structure is modeled as 2-D frame, as shown in Fig. 2(b), and the non-stationary seismic responses are calculated. Fig. 3(a) shows the contour map of constraint condition 1, $\tilde{F}^b(\omega_b, \mu)$, when $PGA=0.5$ g. The thick dashed line indicates the contour line of $F^b(\omega_b, \mu)=5\%$, and the shaded area is the region in which constraint condition 1 is satisfied. Fig. 3(b) is the contour map of the objective function $\tilde{f}_{obj}(\omega_b, \mu)$, the thick dashed line in the figure is the boundary of constraint condition 1. The dotted dashed line is the boundary of constraint condition 2, and the shaded portion is the region where both conditions are satisfied. The '●' is the optimal point of the parameters; the values of the optimized parameters are $[\omega_b^{opt}, \mu^{opt}] = [2.110, 4.776\%]$. It can be seen in the figure that the optimal point is at the boundary

of constraint condition 2, where the bearing has a value of $S_2=5$. Because $S_2 = \frac{D}{ntr}$, the total thickness of the rubber is $ntr = D/5 = 0.14$ m. In addition, $\mu^{opt} = \frac{N(1-\alpha)f_y^{opt}}{M_z g}$, so the optimal yield force of a single bearing is $f_y^{opt} = 150$ kN. When the yield stress of lead is 8.83 MPa, it is found that the diameter of the lead core is 7.3 cm. Fig. 4(a) shows the variation curve of the objective

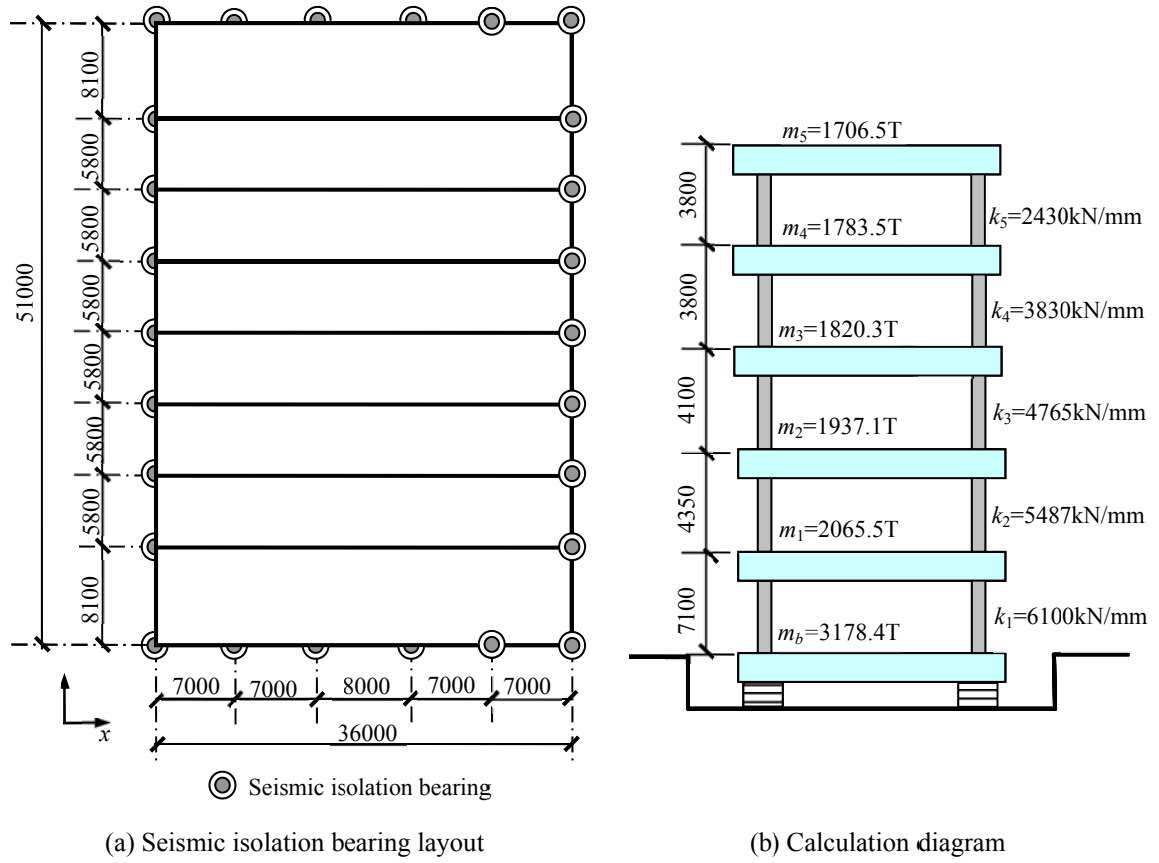


Fig. 2 Seismic isolated structure

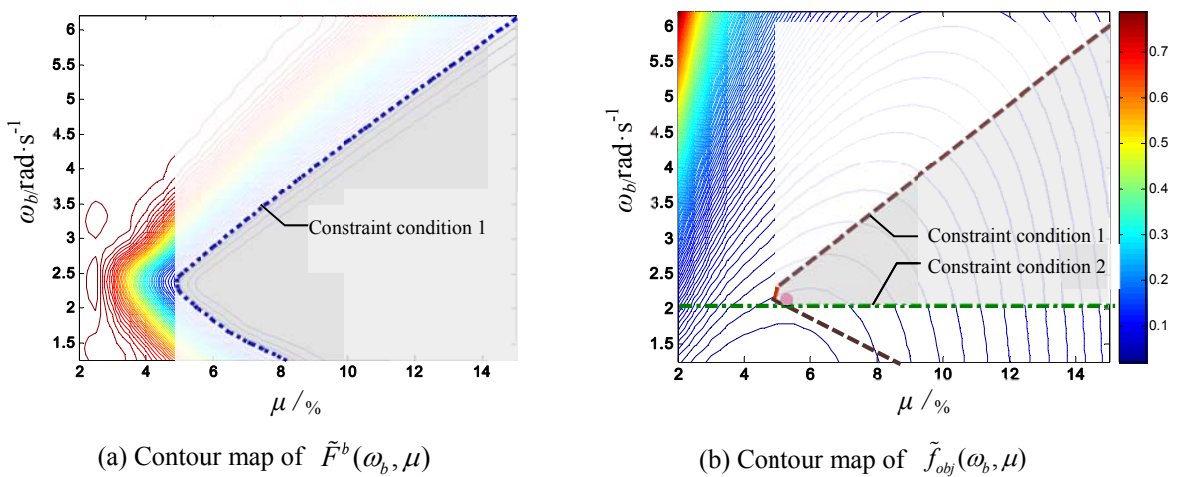
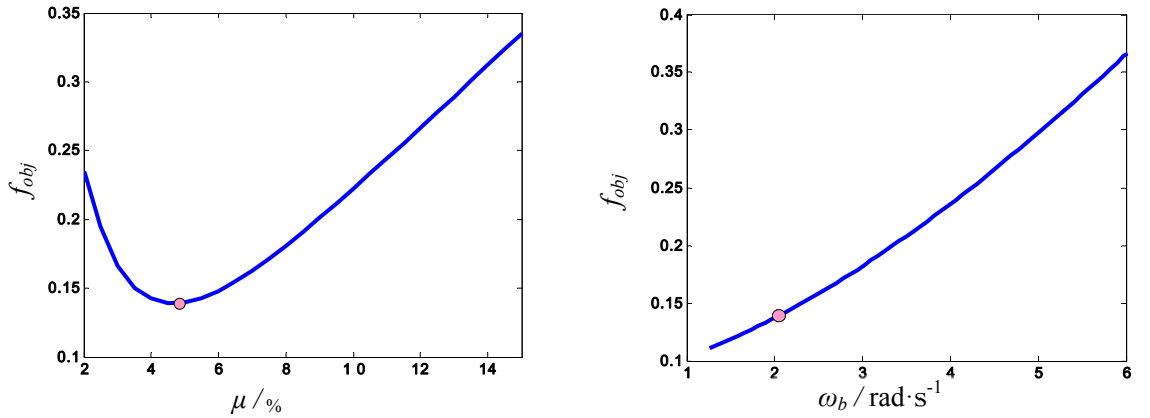


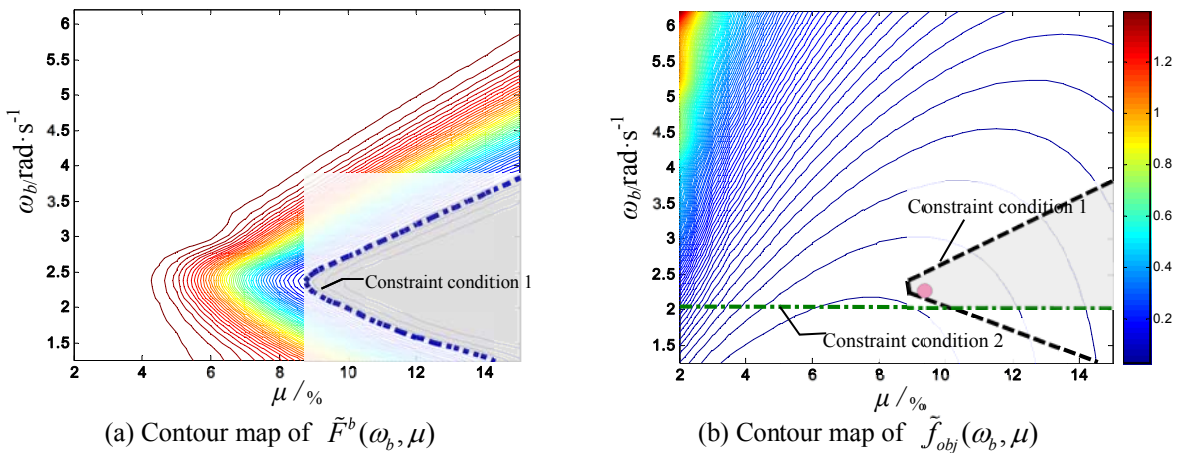
Fig. 3 Contour maps for $\tilde{F}^b(\omega_b, \mu)$ and $\tilde{f}_{obj}(\omega_b, \mu)$ when $PGA=0.5\text{ g}$



(a) Variation curve of $f_{obj}(\omega_b^{opt}, \mu)$ with respect to μ (b) Variation curve of $f_{obj}(\omega_b, \mu^{opt})$ with respect to ω_b

Fig. 4 Variation curves of $f_{obj}(\omega_b^{opt}, \mu)$ with respect to μ and ω_b

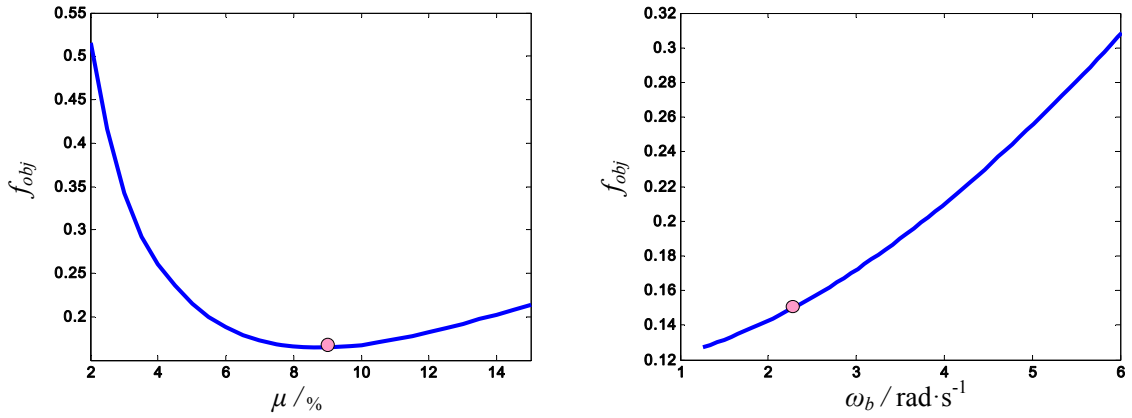
function $f_{obj}(\omega_b^{opt}, \mu)$ with respect to μ when $\omega_b = \omega_b^{opt}$. The figure indicates that the objective function has its minimum value ('•' in the figure) when $\mu = \mu^{opt} = 4.776\%$. Fig. 4(b) shows the variation curve of the objective function $f_{obj}(\omega_b, \mu^{opt})$ with respect to ω_b when $\mu = \mu^{opt}$, indicating that $f_{obj}(\cdot)$ monotonously decreases with the decrease in ω_b . However, when $\omega_b < \omega_b^{opt}$, constraint condition 2 is not satisfied (that is, $S_2 < 5$), so the solution does not meet the stability requirement. Figs. 5(a) and (b) are the contour maps of $\tilde{F}^b(\omega_b, \mu)$ and $\tilde{f}_{obj}(\omega_b, \mu)$ when $PGA=0.8$ g. Comparison of Figs. 5 and 6 indicates that when PGA increases, the allowable region for the bearing design parameters decreases, i.e., the shaded area that satisfies the constraint conditions decreases. Fig. 5 shows that the actual values of the optimized parameters are $[\omega_b^{opt}, \mu^{opt}] = [2.203, 9.43\%]$, and it shows that the optimal point is at the boundary of constraint



(a) Contour map of $\tilde{F}^b(\omega_b, \mu)$

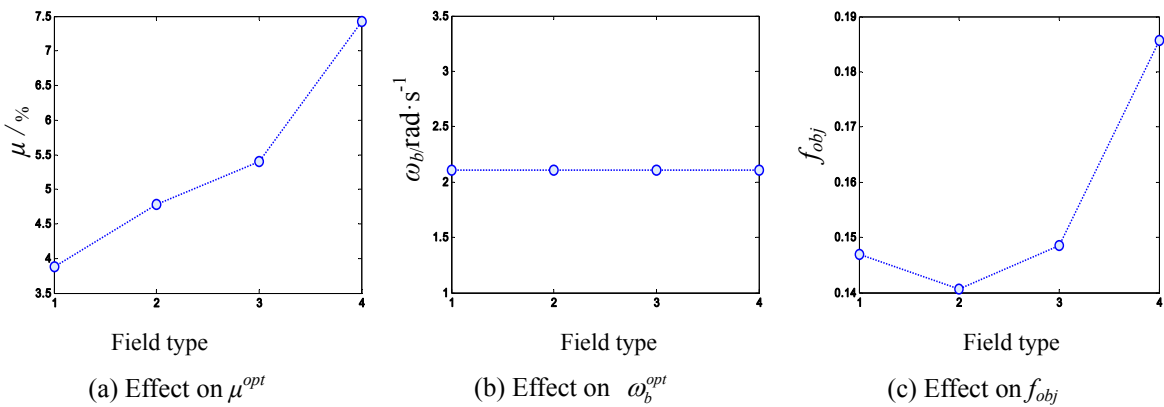
(b) Contour map of $\tilde{f}_{obj}(\omega_b, \mu)$

Fig. 5 Contour maps for $\tilde{F}^b(\omega_b, \mu)$ and $\tilde{f}_{obj}(\omega_b, \mu)$ when $PGA=0.8$ g



(a) Variation curve of $f_{obj}(\omega_b^{opt}, \mu)$ with respect to μ (b) Variation curve of $f_{obj}(\omega_b, \mu^{opt})$ with respect to ω_b

Fig. 6 Variation curves of $f_{obj}(\omega_b^{opt}, \mu)$ with respect to μ and ω_b



(a) Effect on μ^{opt}

(b) Effect on ω_b^{opt}

(c) Effect on f_{obj}

Fig. 7 Effects of field soil type on μ^{opt} , ω_b^{opt} , and f_{obj}

condition 1, above constraint condition 2, i.e., where $S_2 > 5$. According to Eq. (25), the total thickness of the rubber is 0.128 m, the optimal yield force of a single bearing is $f_y^{opt} = 296$ kN and the diameter of the lead core is 10 cm. Figs. 6 (a) and (b) show the variation curves of the objective function $\tilde{f}_{obj}(\omega_b, \mu)$ when $\omega_b = \omega_b^{opt}$ and $\mu = \mu^{opt}$ with respect to μ and ω_b , respectively. When $\mu = \mu^{opt}$, $f_{obj}(\omega_b^{opt}, \mu)$ reaches its minimum value. The objective function $f_{obj}(\omega_b, \mu^{opt})$ monotonically decreases with decreasing ω_b , but when $\omega_b < \omega_b^{opt}$, constraint condition 1 is not satisfied, indicating that an excessive displacement of the bearing will occur.

7.2 Impact of various factors on the optimal parameters of the bearing

7.2.1 Field soil type

The conditions are set as follows: the input seismic ground motion is $PGA = 0.5$ g, the bearing rubber has a shore hardness of 45 degrees, the shear modulus is $G = 0.54$ MPa, the bearing diameter is $D = 0.7$ m and the m value for constraint condition 2 is 5, i.e., $S_2 \geq 5$. Figs. 7(a)-(c) show the

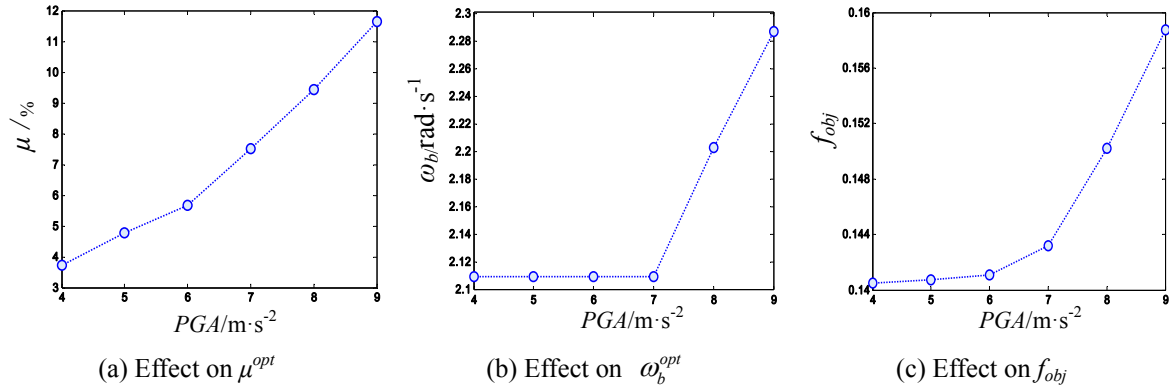


Fig. 8 Effects of PGA on μ^{opt} , ω_b^{opt} , and f_{obj}

optimal bearing parameters ω_b^{opt} and μ^{opt} and the objective function value f_{obj} for different site soil types (see Table 1 for the corresponding seismic ground motion parameters associated with various field soil types). Based on the figure, it can be seen that the softer the field, the greater the optimal yield force of the bearing, μ^{opt} . However, the ω_b^{opt} of the bearings in all types of soil has the same value: 2.110. This indicates that the corresponding second shape factor of the bearing is $S_2=5$. Based on Fig. 7(c), it can be seen that the isolation performance of the isolated structure in a hard field is superior to that in a soft field.

7.2.2 PGA value

The conditions are set as follows: the bearing rubber has a shore hardness of 45 degrees, the shear modulus is $G=0.54$ MPa, the bearing diameter is $D=0.7$ m, the field soil is type II and the m value for constraint condition 2 is 5, i.e., $S_2 \geq 5$. Figs. 8(a)-(c) show the effects of PGA of ground motion on ω_b^{opt} and μ^{opt} and on the objective function value f_{obj} . It can be seen that the value of ω_b^{opt} is 2.110 when $PGA \leq 0.7g$, and the corresponding second form factor of the bearing is $S_2=5$. When $PGA > 0.7g$, ω_b^{opt} increases with increasing PGA, and μ^{opt} increases monotonically with increasing PGA. That is, the higher the PGA value is, the higher the optimal bearing yield force. Based on Fig. 8(c), it can be seen that the isolation effect decreases as PGA increases.

7.2.3 M value

The conditions are set as follows: the input seismic ground motion is $PGA=0.5g$, the bearing rubber has a shore hardness of 45 degrees, the shear modulus is $G=0.54$ MPa, the bearing diameter is $D=0.7$ m and the field soil is type II. Figs. 9(a)-(c) show the optimal bearing parameters ω_b^{opt} and μ^{opt} , as well as the objective function value f_{obj} , for different values of m . Based on the figure, it can be seen that ω_b^{opt} , μ^{opt} and the value of objective function decrease as m decreases. This indicates that the lower the minimum limit of S_2 is, the better the isolation performance of the isolated structure. Therefore, to improve the isolation results, one can try to increase the stability of the bearing and thus decrease the value of m .

7.2.4 Bearing diameter

The conditions are set as follows: the input seismic ground motion is $PGA=0.5g$, the bearing

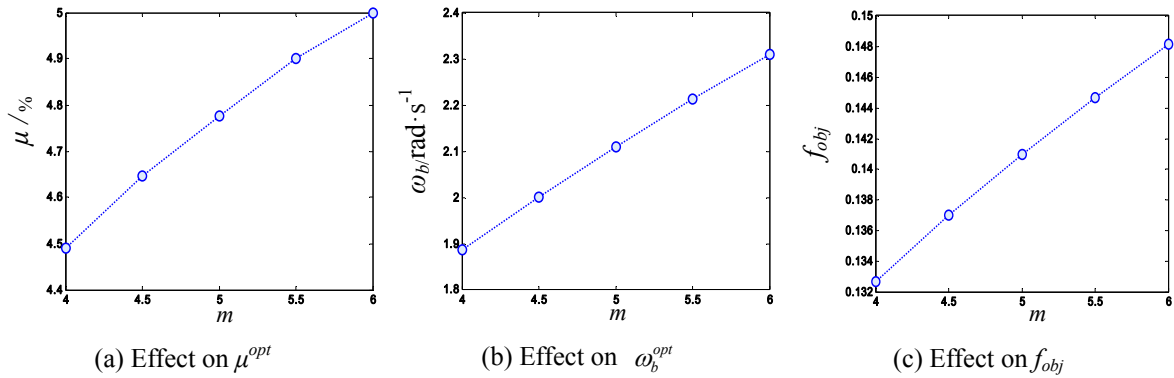


Fig. 9 Effects of m on μ^{opt} , ω_b^{opt} , and f_{obj}

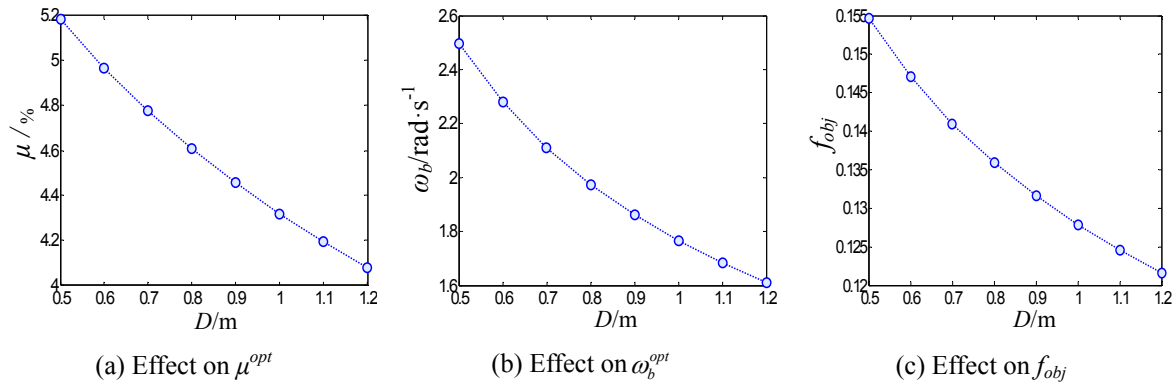


Fig. 10 Effects of bearing diameter on μ^{opt} , ω_b^{opt} , and f_{obj}

rubber has a shore hardness of 45 degrees, the shear modulus is $G=0.54$ Mpa, the field soil is type II and the m value for constraint condition 2 is 5, i.e., $S_2 \geq 5$. Figs. 10(a)-(c) show the impact of bearing diameter D on ω_b^{opt} , μ^{opt} and f_{obj} , respectively. The figure shows that the values of ω_b^{opt} , μ^{opt} and f_{obj} all decrease with increasing D . This indicates that the larger the bearing diameter is, the better the isolation effect of the bearing and the smaller the optimal frequency and optimal yield force of the isolated structure. Therefore, in actual engineering projects, one should try to choose a diameter of the bearing that is as large as possible.

7.2.5 Shore hardness of the rubber

The conditions are set as follows: the input seismic ground motion is $PGA=0.5$ g, the bearing diameter is $D=0.7$ m, the field soil is type II and the m value for constraint condition 2 is 5, i.e., $S_2 \geq 5$. Figs. 11(a)-(c) show the effects of shore hardness on ω_b^{opt} , μ^{opt} and f_{obj} , respectively. Based on the figure, it can be seen that ω_b^{opt} , μ^{opt} and f_{obj} decrease as the Shore hardness of the rubber increases, indicating that the softer the rubber is, the better the isolation effect of the isolated structures and the smaller the optimal frequency and optimal yield force. Thus, it is recommended that softer rubber should be used when the vertical stiffness of the bearing meets the requirement.

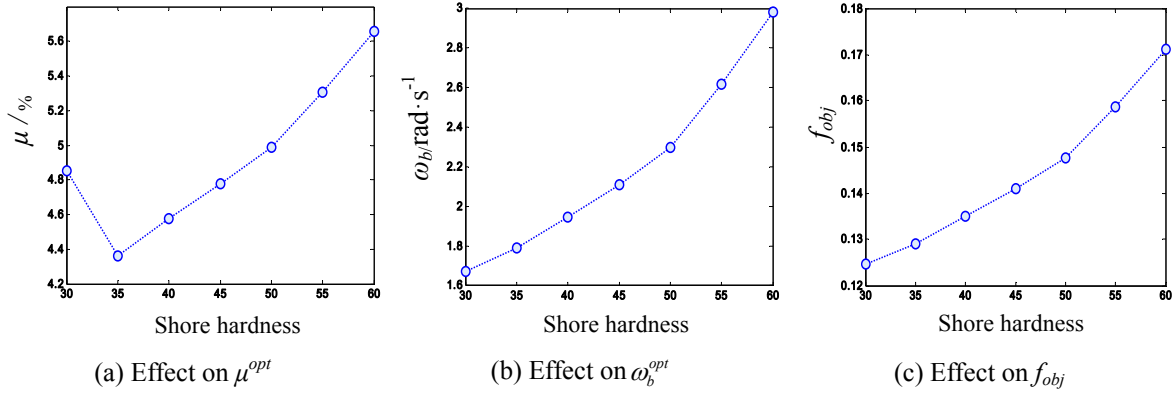


Fig. 11 Effects of shore hardness on μ^{opt} , ω_b^{opt} , and f_{obj}

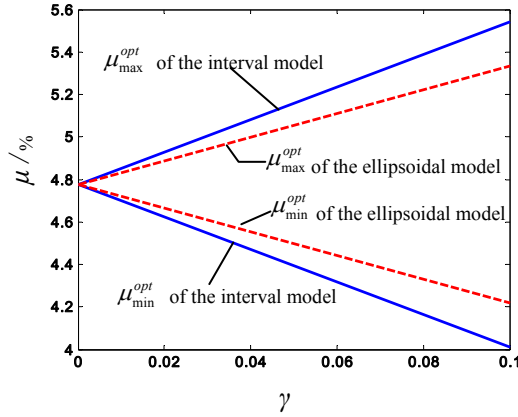


Fig. 12 Value range of μ^{opt} when the deviation rate γ varies between 0 and 10%

7.3 Impact of uncertainty on the optimization of bearing parameters

The uncertainties of the earthquake ground motion parameters and structural parameters are listed in Table 2. The averages of the peak values of acceleration of the ground motions are all 0.5g. The field soil is type II, and the corresponding values of ω_g^c , ω_f^c , ξ_g^c and ξ_f^c are listed in Table 1. The values of structural parameters K^c , M^c and m_b^c are shown in Fig. 2(b). The bearing diameter is 0.7 m, the rubber shore hardness is 45 degrees, the shear modulus is 0.54 MPa and $m=5$ for constraint condition 2. As is discussed above, the optimal ω_b^{opt} value is found at the boundary of constraint condition 2, i.e., $S_2=m=5$. Therefore, the total rubber thickness is $ntr=D/S_2=0.14$ m. Taking into account only the effects of uncertainty parameters on μ^{opt} and using Eq. (35), the following Taylor expansion of $\mu^{opt}(\delta)$ at $\delta=0$ can be obtained:

$$\tilde{\mu}^{opt}(\delta) = 4.776 + 0.00864\delta_1 - 0.00897\delta_2 - 0.0221\delta_3 - 0.233\delta_4 + 0.494\delta_5$$

In the above equation, the value of the coefficient $\frac{\partial \mu^{opt}(\mathbf{0})}{\partial \delta_i}$ reflects the different effects of the uncertainties of different parameters on μ^{opt} . It can be seen that μ^{opt} increases as δ_1 and δ_5 increase, and it decreases with increasing $\delta_2, \delta_3, \delta_4$. The parameter δ_5 has the greatest effect on μ^{opt} , followed by $\delta_4, \delta_3, \delta_2$ and δ_1 . Therefore, the uncertainties of the seismic ground motion parameters have a greater impact than the uncertainties of the structural parameters. Substitution of the above equation into Eq. (34) allows us to obtain the value range of μ^{opt} , $[\mu_{min}^{opt}, \mu_{max}^{opt}]$, by either using the interval model or the ellipsoidal model. Fig. 12 shows the value range of μ^{opt} when the deviation rate between 0 and 10%. The figure shows that the value range of μ^{opt} increases with increasing parameter deviation. Because the ellipsoidal model takes into account the partial correlation between the uncertainties of parameters, the resulting range of μ^{opt} is narrower than that derived from the interval model. In actual design practice, when the parameter uncertainties are considered, one should choose the upper limit of μ^{opt} (μ_{max}^{opt}) as a design value.

7. Conclusions

In this paper, an optimization method is proposed for mechanical parameters for the design of lead-core rubber bearings system subjected to non-stationary earthquake ground motions. In this method, the post-yielding stiffness and normalized yield force are used as design variables, the minimum value of the maximum energy response level of the upper structure during an earthquake is used as an objective function, and the constraint conditions include the probability of bearing failure not exceeding 5% and the second shape factor of the bearing being less than 5. By combining the RBF response surface method and the SQP algorithm, the optimization problem could be solved, and the optimal values could be provided for the design variables. Furthermore, an interval model and ellipsoidal model can be applied to describe the uncertainties of structural and seismic ground motion parameters. Subsequently, the upper and lower limits of the optimal values for the bearing design parameters can be determined by using a first-order Taylor series expansion and the Lagrange multiplier method. Through the calculation of an example, the following results can be obtained:

(1) When the *PGA* of the input seismic ground motion is relatively small, i.e., $PGA \leq 0.7$ g, the optimal second shape factor of the bearing is $S_2^{opt} = m$ (m is the minimal value required to prevent bearing vertical instability, usually in the range of 4 - 6). When *PGA* is relatively large, i.e., $PGA > 0.7$ g, S_2^{opt} is slightly greater than m . Moreover, the optimal normalized yield force μ^{opt} increases with increasing *PGA*.

(2) The field soil type affects the optimal normalized yield force of the bearing (μ^{opt}). The softer the field is, the higher the value of μ^{opt} . Isolated structures in soft fields have worse isolation performance than they do in hard fields.

(3) The larger the bearing diameter is, the lower the value of μ^{opt} and the better the isolation performance of the isolated structure. Therefore, bearings with larger diameter are recommended in actual engineering projects.

(4) The lower the shore hardness of the rubber in the bearings is, the smaller the value of μ^{opt} and the better the isolation performance of the isolated structures. Therefore, softer rubber is recommended in practice.

Acknowledgments

The research described in this paper was financially supported by the NSFC (National Natural Science Foundation of China), project No. 51078166 and No. 51278213.

References

- Chaudhuri, A. and Chakraborty, S. (2004), "Sensitivity evaluation in seismic reliability analysis of structures", *Comput. Meth. Appl. Mech. Eng.*, **93**, 59-68.
- Baratta, A. and Corbi, L. (2004), "Optimal design of base-isolators in multi-storey buildings", *Comput. Struct.*, **82**, 2199-209.
- Ben-Haim, Y. (1994), "A non-probabilistic concept of reliability", *Struct. Saf.*, **16**(4), 227- 245.
- Bucher, C. (2009), "Probability-based optimal design of friction-based seismic isolation devices", *Struct. Saf.*, **31**, 500-507.
- Clough, R.W. and Penzien, J. (1977), *Dynamics of structures*, McGraw-Hill Inc, New York, NY, USA.
- Constantinou, M.C. and Tadjbakhsh, I.G. (1984), "Optimum design of a base isolation system with frictional elements", *Earthq. Eng. Struct. Dyn.*, **12**, 203-14.
- Dicleli, M. and Karalar, M. (2011), "Optimum characteristic properties of isolators with bilinear force-displacement hysteresis for seismic protection of bridges built on various site soils", *Soil Dyn. Earthq.*, **31**, 982-995.
- Ellishakoff, I. (1995), "Essay on uncertainties in elastic and viscoelastic structures: from AM Freudenthal's criticisms to modern convex modeling", *Comput. Struct.*, **56**(6), 871 - 895.
- Fang, H. and Horstemeyer, M.F. (2006), "Global response approximation with radial basis functions", *Eng. Optim.*, **38**, 407-424.
- Gur, S. and Mishra, S.K. (2013), "Multi-objective stochastic-structural-optimization of shape-memory-alloy assisted pure-friction bearing for isolating building against random earthquakes", *Soil Dyn. Earthq.*, **54**, 1-16.
- Iemura, H., Taghikhany, T. and Jain, S.K. (2007), "Optimum design of resilient sliding isolation system for seismic protection of equipments", *B. Earthq. Eng.*, **5**, 85-103.
- Islam, A.B.M.S., Hussain, R.R., Jameel, M. and Jumaat, M.Z. (2012), "Non-linear time domain analysis of base isolated multi-storey building under site specific bi-directional seismic loading", *Automat. Constr.*, **22**, 554-566.
- Jangid, R.S. (2005), "Optimum friction pendulum system for near-fault motions", *Eng. Struct.*, **27**, 349-59.
- Jangid, R.S. (2007), "Optimum lead-rubber isolation bearings for near-fault motions", *Eng. Struct.*, **29**, 2503-13.
- Jangid, R.S. (2008), "Equivalent linear stochastic seismic response of isolated bridges", *J. Sound Vib.*, **309**, 805-22.
- Jennings, P.C. and Housener, G.W. (1968), "Simulated earthquake motions for design purpose", *Proceedings of the 4th World Conference on Earthquake Engineering*, Santiago, Chile.
- Jensen, H.A. (2005), "Design and sensitivity analysis of dynamical systems subjected to stochastic loading", *Comput. Struct.*, **83**, 1062-75.
- Marano, G.C., Greco, R. and Morrone, E. (2011), "Analytical evaluation of essential facilities fragility curves by using a stochastic approach", *Eng. Struct.*, **33**, 191-201.
- McDonald, D.B., Grantham, W.J. and Tabor, W.L. (2007), "Global and local optimization using radial basis function response surface models", *Appl. Math. Model.*, **31**, 2095-2110
- Mishra, S.K. and Chakraborty, S. (2013), "Performance of a base-isolated building with system parameter uncertainty subjected to a stochastic earthquake", *Int. J. Acoust. Vib.*, **18**(1), 7-19.
- Mishra, S.K., Roy, B.K. and Chakraborty, S. (2013), "Reliability-based-design-optimization of base isolated buildings considering stochastic system parameters subjected to random earthquakes", *Int. J. Mech. Sci.*,

- 75, 123-33.
- Ozbulut, O.E. and Hurlebaus, S. (2011), "Optimal design of superelastic-friction base isolators for seismic protection of highway bridges against near-field earthquakes", *Earthq. Eng. Struct. Dyn.*, **40**, 273-91.
- Park, J.G. and Otsuka, H. (1999), "Optimal yield level of bilinear seismic isolation devices", *Earthq. Eng. Struct. Dyn.*, **28**, 941-55.
- Pourzeynali, S. and Zarif, M. (2008), "Multi-objective optimization of seismically isolated high-rise building structures using genetic algorithms", *J. Sound Vib.*, **311**, 1141-60.
- Qiu, Z. and Wang, J. (2010), "The interval estimation of reliability for probabilistic and non-probabilistic hybrid structural system", *Eng. Fail. Anal.*, **17**(5), 1142-1154.
- Schueller, G.I. and Jensen, H.A. (2008), "Computational methods in optimization considering uncertainties-an overview", *Comput. Meth. Appl. Mech. Eng.*, **198**(1), 2-13.
- Vanmarcke, E.H. (1975), "On distribution of the first-passage time for normal stationary random processes", *J. Appl. Mech.*, **42**, 215-20.
- Zou, X.K. (2008), "Integrated design optimization of base-isolated concrete buildings under spectrum loading", *Struct. Multidiscip. O.*, **36**, 493-507.

Appendix

$$A_e(t) = \begin{bmatrix} \mathbf{O}_{(n+1)(n+1)} & \mathbf{O}_{(n+1) \times 1} & \mathbf{O}_{(n+1) \times 1} & \mathbf{I}_{(n+1)(n+1)} & \mathbf{O}_{(n+1) \times 1} & \mathbf{O}_{(n+1) \times 1} \\ \mathbf{O}_{1 \times (n+1)} & 0 & 0 & \mathbf{O}_{1 \times (n+1)} & 1 & 0 \\ \mathbf{O}_{1 \times (n+1)} & 0 & 0 & \mathbf{O}_{1 \times (n+1)} & 0 & 1 \\ -(M^{-1}K)_{(n+1) \times (n+1)} & (M^{-1}I_m \omega_f^2)_{(n+1) \times 1} & -(M^{-1}I_m \omega_g^2)_{(n+1) \times 1} & -(M^{-1}C)_{(n+1) \times (n+1)} & (M^{-1}I_m \cdot 2\xi_f \omega_f)_{(n+1) \times 1} & (M^{-1}I_m \cdot 2\xi_g \omega_g)_{(n+1) \times 1} \\ \mathbf{O}_{1 \times (n+1)} & -\omega_f^2 & \omega_g^2 & \mathbf{O}_{1 \times (n+1)} & -2\xi_f \omega_f & 2\xi_g \omega_g \\ \mathbf{O}_{1 \times (n+1)} & 0 & -\omega_g^2 & \mathbf{O}_{1 \times (n+1)} & 0 & -2\xi_g \omega_g \end{bmatrix}$$

$$F(t) = [0, 0, \dots, 0, -a(t)w(t)]_{2(n+3) \times 1}^T$$